Synthesis of nanoscale CN_x/TiAlN multilayered coatings by ion-beam-assisted deposition

M. Cao, D. J. Li,[a] and X. Y. Deng
College of Physics and Electronic Information Science, Tianjin Normal University, Tianjin 300387, China

X. Sun
Department of Mechanical and Materials Engineering, University of Western Ontario, London, Ontario, Canada N6A 5B9

(Received 2 November 2007; accepted 16 June 2008; published 28 August 2008)

CN_x/TiAlN multilayered coatings with different nanoscale modulation periods and ratio of CN_x within each period were prepared by ion-beam-assisted deposition at room temperature. Auger electron spectroscopy (AES), x-ray diffraction (XRD), and nanoindenter and a profiler were used to characterize the microstructure and mechanical properties of the coatings. The low-angle XRD pattern and AES indicated a well-defined multilayered structure of the coating. Although monolithic CN_x and TiAlN coatings formed amorphous and nanocrystalline structures, respectively, the CN_x/TiAlN multilayers exhibited coherent epitaxial growth due to the mutual growth-promoting effect at small CN_x layer thickness (<0.6 nm). At modulation period $\Lambda=2.83$ nm and CN_x thickness of 10% within each period, the multilayers exhibited strong TiAlN (111) and weak AlN (111) textures and showed the highest hardness (32 GPa), elastic modulus (409 GPa), and critical fracture load (65.7 mN). © *2008 American Vacuum Society.* [DOI: 10.1116/1.2956627]

I. INTRODUCTION

The growth and characterization of multilayered structures have attracted considerable attention from both the scientific and industrial communities in recent years[1] because of their promising properties.[2] These structures consist of repeating layers of two different materials with nanoscale dimensions. The thickness of each successive pair of layers is commonly known as the modulation period (Λ), which critically affects the multiplayer properties.[3] Much of the work on nanolayered structures has focused on nitride-based materials for superhard protective coatings[4] and other wear-resistance applications.[5] Several new material systems, including TiAlN/TiN, CrN/TiN, and ZrN/WN, exhibit enhanced microhardness.[6–8]

On the other hand, recent studies show that nonequilibrium structures can be presented in very thin layers in nanomultilayers, a so-called epitaxial stabilization effect. Such an epitaxial stabilization effect can also be used to seed amorphous to crystallize transitions. For example, less than 1-nm-thick crystalline SiC, SiO_2, and TiB_2 were found to be forced to crystallize due to the template effect of TiN.[9–11] In these multilayers, the crystallization of amorphous layers was able to significantly improve the film's mechanical properties.

TiAlN is a favorite because it has a reputation for being wear resistant and chemically stable at high working temperature.[12] Ion-beam-assisted deposition (IBAD) films of CN_x are usually amorphous. Nevertheless, if a template is provided to seed CN_x growth, it might form a crystalline structure and consequently cause a novel enhancement in the film's mechanical properties. The aim of this work is to deposit CN_x/TiAlN multilayered coatings with different nanoscale modulation periods and ratio of CN_x within each period using our IBAD system. Our purpose is to obtain insight into the significance of layered structures on the properties of CN_x/TiAlN multilayered coatings.

II. EXPERIMENT

An IBAD system with two ion sources, one rotatable water-cooled sample holder, and one rotatable water-cooled target holder was used to synthesize CN_x/TiAlN multilayered coatings. Through computer control, we could rotate C and Ti(50%)Al(50%) targets to the sputtered working position and alternate time-C expose the targets to the sputtering Ar^+ beam to obtain different modulation periods. Before deposition, a silicon (100) substrate was cleaned for 5 min with a 500 eV, 5 mA Ar^+ beam from a low-energy ion source. The introduction of Ar, N_2 to two ion sources was controlled independently using mass-flow controllers. C and TiAl targets were sputtered alternately by Ar^+ beam (1.4 keV and 25 mA) from a sputtering ion source to deposit C or TiAl coatings. The resulting coatings were simultaneously bombarded by a N^+ beam (200 eV and 5 mA) from low energy on the source to synthesize CN_x/TiAlN multilayered coatings. Depositions were made at room temperature. The base pressure was better than 3.0×10^{-4} Pa, with a working pressure of about 2.0×10^{-2} Pa. All coatings were grown to a thickness of 400 nm.

An XP-2 profiler was used to measure thickness and curvature of the CN_x/TiAlN coatings to calculate residual stress. X-ray diffraction (XRD) (D/MAX 2500) with Cu $K\alpha$ radiation at 1.540 56 Å was employed for the coating structure. The element compositions and depth profiles of the coatings were investigated by the surface-sensitive Auger

[a]Author to whom correspondence should be addressed; Tel.: +86-22-23766519; electronic mail: dejunli@mail.tjnu.edu.cn

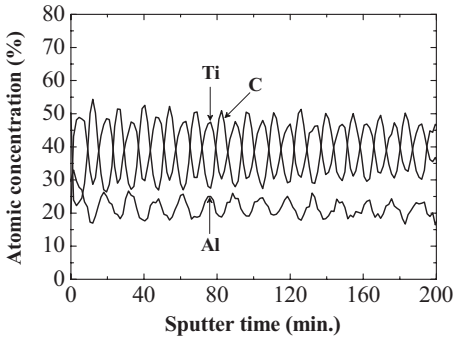

FIG. 1. Sputter depth profile of the CN_x/TiAlN multilayer with $\Lambda = 12.5$ nm.

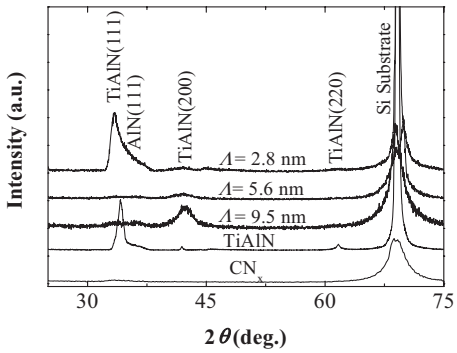

FIG. 3. High-angle XRD patterns of CN_x/TiAlN coatings with different Λ.

electron spectroscopy (AES) with a PHI model P660 scanning Auger microscopy system. In this measurement, the electron-beam accelerating voltage was 5 kV, used to excite Auger electron emission from the sample surface. An Ar^+ sputter gun was at 3 kV, with a raster area of 4.0 $\times$4.0 mm^2. The hardness and elastic modulus of the coatings as a continuous function of depth from a single indentation were obtained by the continuous stiffness measurement (CSM) technique using a nanoindenter XP system. This system was also used to perform the nanoscratch test. In this test, the maximum load was up to 100 mN to measure the fracture resistance.

III. RESULTS AND DISCUSSION

A series of CN_x/TiAlN multilayered coatings were synthesized in different modulation periods at the ratio of CN_x of 15% within each period. The multilayered architecture is illustrated by the AES composition depth profile in Fig. 1. The concentrations of Ti, Al, and C as the main elements in the coating showed periodic variation throughout the thickness. Ti and Al elements showed a consistent variation and C showed an opposite trend. This is apparently a result of the alternating materials of CN_x and TiAlN. The atomic composition of Ti/Al was about 2:1 within the TiAlN layer because of ion-beam selective sputtering of the TiAl alloy target.

The low-angle XRD patterns of Fig. 2 indicate the nature of the nanoscale multilayered structure of the multilayers. The numerous reflections indicate a sharp interface between the CN_x and TiAlN layers. Their periods were calculated to be 2.8, 5.6, and 9.5 nm from the orientation peaks using the modified Bragg equation.

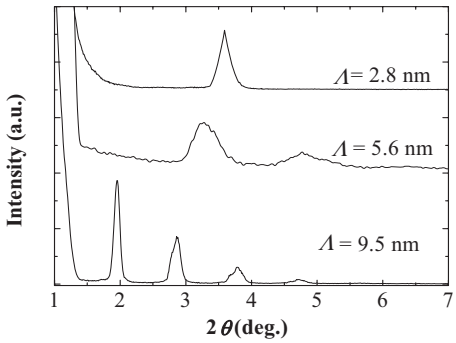

FIG. 2. Low-angle XRD patterns for CN_x/TiAlN coatings with different Λ.

Figure 3 shows the high-angle XRD patterns obtained from CN_x, TiAlN, and CN_x/TiAlN multilayer coatings with different Λ under identical deposition conditions. It was clear that the monolithic CN_x coating showed an amorphous character. Three broadened peaks were found at about 35°, 43°, and 62° in the TiAlN coating, so the face-centered-cubic (fcc) phase of TiAlN was identified. A strong TiAlN (111) peak and weak TiAlN (200) and (220) texture were observed. At the same time, AlN (111) (fcc) was also found in the TiAlN coating. However, in multilayered coatings, when Λ was 2.8 nm, the CN_x/TiAlN multilayer presented a very strong (111) texture. Detailed crystal structure information of the CN_x layer is difficult to obtain due to layer's thickness. So, we speculate that the CN_x layer only several atomic layer thick formed a fcc structure due to the template effect of TiAlN when CN_x was limited to less than 0.6 nm. Figure 3 also indicates that with increased thickness of the CN_x layer, the diffraction intensity of the (111) peak decreased rapidly and multilayers gradually presented (200) texture. We can speculate that CN_x gradually transformed from an epitaxial cubic structure to amorphous when its thickness was more than 0.6 nm, and impeded the coherent epitaxial growth of multilayers. As a result, crystal defects appeared in these multilayers and the coherent growing structure was gradually destroyed. When Λ was more than 9.5 nm, the deposited TiAlN particles renucleated on the amorphous CN_x layer and grew with (200) texture. Multilayers presented a modulated structure composed of amorphous CN_x and nanocrystal TiAlN.

A series of CN_x/TiAlN multilayered coatings was synthesized at different CN_x ratios within each Λ of 2.8 nm. Figure 4 shows that the intensity of sharp (111) peaks decreased and then disappeared with increasing the ratio of CN_x from 10% to 30%. At the ratio of CN_x of 10%, the CN_x layer promoted the crystal growth of the TiAlN layer and strengthened (111) diffraction peak. With an increasing ratio of CN_x, the CN_x layers transformed the TiAlN to an amorphous structure, which blocks the coherent growth of the coatings. Crystalli-

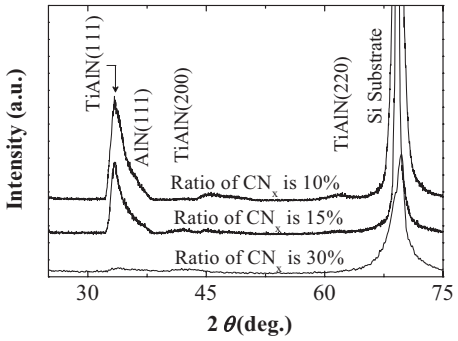

FIG. 4. High-angle XRD patterns of CN_x/TiAlN coatings with different ratios of CN_x.

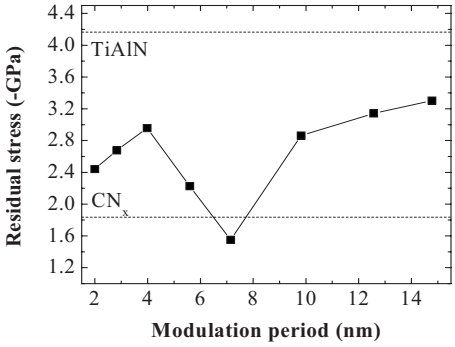

FIG. 5. Residual stress of the CN_x/TiAlN coatings vs Λ.

zation and coherent growth for multilayered coatings with a smaller CN_x layer may cause a positive effect on its mechanical properties.

From XRD patterns, our results are consistent with some similar findings in other multilayers, such as TiN/SiC,[9] TiN/SiO_2,[10] and ZrN/Si_3N_4.[13] Some theories are used to analyze the growth of nanoscale multilayered coatings consisting of amorphous and polycrystalline layers.[10,13] This crystallization and coherent growth for multilayered coatings with a smaller CN_x layer can be explained by thermodynamics and kinetics.[13] At the early stages of layer nucleation, CN_x can grow with a structure that matches well the structure of fcc TiAlN, and forms coherent layer interfaces to minimize interfacial energy. With increasing thickness, the CN_x layer gradually transform typically from epitaxial cubic structure to amorphous. In addition, the character of the growing surface has an influence on the mobility of deposited particles. TiAlN and CN_x particles form nanocrystalline and amorphous structures during deposition, respectively, due to low mobility. In multilayers, however, due to the different characters and structures of growing surfaces, TiAlN and CN_x particles have higher mobility. Therefore, the integrity of the crystal growth of multilayers improves and the columnar grains with intensive preferred orientation are found in the multilayers.

Residual stress is a key parameter affecting industrial applications of protective coatings because higher residual stress is the main reason of coating delamination and plastic deformation. Its value can be calculated applying the Stoney formula[14] and using the substrate curvature determined by a surface profiler

$$\sigma = -\frac{E_s t_s^2}{6t_c(1-v_s)R},$$

with E_s, t_s, and v_s being, respectively, elastic modulus, thickness, and Poisson's ratio of the substrate. t_c is the coating thickness and R is the radius of curvature of the multilayer coated substrate. The residual stresses of the multilayered coatings versus modulation periods are shown in Fig. 5. Monolithic TiAlN coating possesses high residual stress, i.e., compressive stress of 4.2 GPa. All multilayered coatings have lower compressive stress than the average value of the two monolithic TiAlN and CN_x coatings. The coating with about 5–8 nm periods shows the lower stress. The stress decreases sharply with increasing the ratio of CN_x within identical Λ of 2.8 nm observed in Fig. 6. These results indicate that compressive stress depends strongly on modulation period and ratio of CN_x during multilayer growth.

The residual stress of multilayered coatings increases with modulation periods at the start of the growth processing, because the CN_x layer gradually produces an epitaxial cubic structure mentioned above. For modulation periods over 4 nm, the CN_x layer gradually transforms to amorphous, relaxing the stress built in the TiAlN layers. So CN_x/TiAlN coatings with 5–8 nm periods show the lower stress. However, when Λ is greater than 10 nm, defects in volume are difficult to diffuse to or cross CN_x/TiAlN interfaces, so strain fields that build in the TiAlN layers are not easy to relieve. Similarly, to the multilayers with identical Λ of 2.8 nm, with the increase in the thickness of the CN_x layer, CN_x gradually transforms from an epitaxial cubic structure to amorphous, which may allow stress release. We believe that this stress relaxation is related to interdiffusion. A possible mechanism is the ability of defects in volume to more easily diffuse to or cross the CN_x/TiAlN interfaces and to relieve their strain fields easily when diffusion distance is low. So, small Λ multilayers showed lower compressive stress than larger period ones.

Figure 7 shows hardness and elastic modulus of the CN_x/TiAlN coatings versus modulation periods. To compare

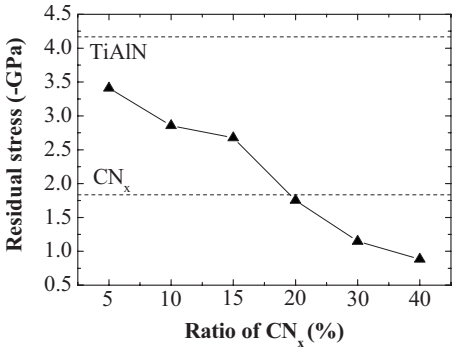

FIG. 6. Residual stress of the CN_x/TiAlN coatings vs the ratio of CN_x when Λ=2.8 nm.

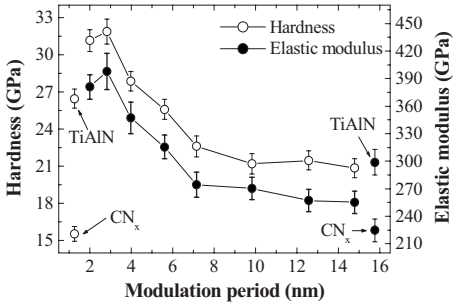

FIG. 7. Hardness and elastic modulus of the CN_x/TiAlN coatings vs Λ.

the multilayers, hardness, and elastic modulus of monolithic TiAlN and CN_x coatings synthesized under identical deposition conditions and identical thickness (about 400 nm) are also shown in this figure. In this test, the method of CSM was used to obtain the hardness and elastic modulus of coatings. This technique allowed the continuous measurement of the contact stiffness during loading. With a continuous measure of stiffness, we obtained the hardness and elastic modulus as a continuous function of depth from a single indentation experiment. The maximum value of hardness and modulus usually appears at 10%–15% of depth of the coating thickness. We chose this value to also minimize substrate effects. The hardness of TiAlN and CN_x are 26.5 and 15.5 GPa, respectively. Multilayered coatings reveal higher hardness in smaller modulation periods. The maximum hardness is up to 32 GPa at $\Lambda=2.8$ nm. After more than 4 nm (CN_x layer >0.6 nm), its value decreases rapidly. The change in the elastic modulus has a similar trend. Figure 8 shows the variations of hardness and elastic modulus versus the ratio of CN_x at fixed $\Lambda=2.8$ nm. The maximum hardness and elastic modulus of 32 and 409 GPa are obtained at the ratio of CN_x of 10% (0.3-nm-thick CN_x layer). It appears that the hardness and the elastic modulus decrease with increasing thickness of CN_x.

The increase in hardness can be understood by examining the XRD data mentioned above. When CN_x is limited to 0.3–0.5 nm, high hardness appears in multilayered coating with a very strong (111) texture due to CN_x layer crystallization and growth coherent and epitaxial with the TiAlN layer. When the CN_x layer is thick, it becames amorphous,

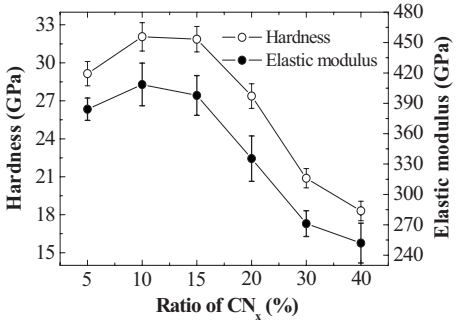

FIG. 8. Hardness and elastic modulus of the CN_x/TiAlN coatings vs the ratio of CN_x when $\Lambda=2.8$ nm.

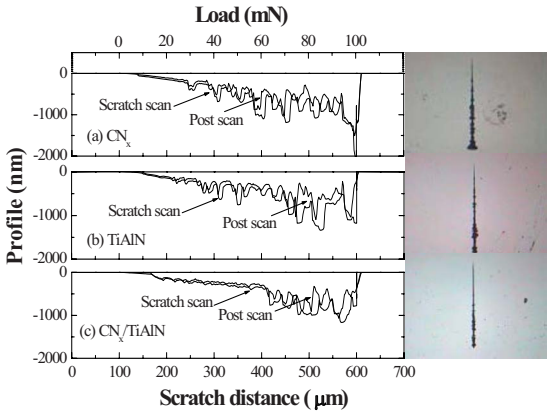

FIG. 9. The scratch-scan and postscan surface profiles and the scratch tracks on the three different coatings.

and the coherent interfaces and epitaxial growth are blocked. Therefore, a sharp decrease in hardness is observed for multilayers. Similar studies showed that the amorphous CN_x,[15] SiC,[9] and SiO_2 [10] crystallized at a thickness of less than 1.0 nm. When they grew coherently with TiN or ZrN layers, multilayers displayed enhanced mechanical properties. These similar findings support our results.

Figure 9 shows the scratch-scan and postscan surface profiles and the scratch tracks on the monolithic CN_x, TiAlN, as well as CN_x/TiAlN coatings synthesized at $\Lambda=2.8$ nm and the ratio of CN_x of 10%. It is reasonable that the postscan curve is always above the scratch-scan curve due to plastic recovery after scratching. All scratch-scan profiles of the coatings indicate an abrupt increase point in scratch depth. The normal load corresponding to this point is the critical fracture load L_c of the coating, characterizing the adhesion strength of the coating. The L_c of CN_x and TiAlN coatings are 29.4 and 36.9 mN, respectively. However, the CN_x/TiAlN coating exhibits smooth scratch-scan and postscan surface profiles and a high L_c value (65.7 mN). Its scratch track also shows better adhesion strength. The adhesion failure is composed of crack initiation and propagation, whereas the crack initiation begins at a flaw that allows stress concentration or bond weakening. We believe that this improved fracture resistance appears to be directly related to low stress, high hardness, and strong plastic recovery of the coating with a multilayered structure.

IV. CONCLUSIONS

The influence of modulation periods and ratios of CN_x on structural and mechanical properties of CN_x/TiAlN coatings was investigated to increase our understanding of multilayered coatings. The CN_x layers were crystallized under the template effects of the crystalline TiAlN layer when their layer thickness was limited to less than about 0.6 nm. At $\Lambda=2.83$ nm and a ratio of CN_x of 10%, the multilayers exhibited a (111)-preferred orientation and showed maximum enhancement of hardness and elastic modulus with values of 32 and 409 GPa, respectively. It also showed lower residual stress value and higher adhesion strength than monolithic

coatings. This work proves that IBAD can produce nanoscale CN_x/TiAlN multilayered coatings with high hardness, high fracture resistance, and low compressive stress by controlling layered structural parameters.

ACKNOWLEDGMENTS

This work was supported by the Key Project of Applied Basic and Advanced Technology Research Plan of Tianjin (2009) and International Collaboration Project of Tianjin Science and Technology Plan (No. 07ZCGHHZ01500). The authors would also like to thank W. H. Chang and W. M. Lau of Surface Science Western, University of Western Ontario, Canada, for their support on this work.

[1]C. J. Tavares, L. Rebouta, B. Almeida, J. Bessa e Sousa, M. F. da Silva, and J. C. Soares, Thin Solid Films **317**, 124 (1998).
[2]P. C. Yashar and W. D. Sproul, Vacuum **55**, 179 (1999).
[3]C. Barshilia and K. S. Rajam, Surf. Coat. Technol. **183**, 174 (2004).
[4]W. D. Sproul, Science **273**, 889 (1996).
[5]K. J. Martin, A. Madan, D. Hoffman, J. Ji, and S. A. Barnett, J. Vac. Sci. Technol. A **23**, 90 (2005).
[6]Q. Luo and P. E. Hovsepian, Thin Solid Films **497**, 203 (2006).
[7]P. Yashar, S. A. Barnett, J. Rechner, and W. D. Sproul, J. Vac. Sci. Technol. A **16**, 2913 (1998).
[8]D. J. Li, M. X. Wang, J. J. Zhang, and J. Yang, J. Vac. Sci. Technol. A **24**, 966 (2006).
[9]M. Kong, J. W. Dai, J. J. Lao, and G. Y. Li, Appl. Surf. Sci. **253**, 4734 (2007).
[10]L. Wei, F. H. Mei, N. Shao, M. Kong, G. Y. Li, and J. G. Li, Appl. Phys. Lett. **86**, 021919 (2005).
[11]F. H. Mei, N. Shao, L. Wei, Y. S. Dong, and G. Y. Li, Appl. Phys. Lett. **87**, 011906 (2005).
[12]S. G. Harris, E. D. Doyle, A. C. Vlasveld, J. Audy, and D. Quick, Wear **254**, 166 (2003).
[13]Y. S. Dong, W. J. Zhao, J. L. Yue, and G. Y. Li, Appl. Phys. Lett. **89**, 121916 (2006).
[14]M. Ohring, *The Materials Science of Thin Films* (Academic, New York, 1992), p. 416.
[15]M. L. Wu, X. W. Lin, V. P. David, Y. W. Chung, M. S. Wong, and W. D. Sproul, Thin Solid Films **308–309**, 113 (1997).